International Journal of Fluid Power 8 (2007) No. 3 pp. 13-23

FLOW CONTROL FOR COORDINATED MOTION AND HAPTIC FEEDBACK

Matthew E. Kontz[1] and Wayne J. Book[2]

[1] *Caterpillar Inc. – Hydraulics Research, Peoria, IL, USA*
[2] *Georgia Institute of Technology – G.W. Woodruff School of Mechanical Engineering, Atlanta, GA, USA*
Kontz_Matthew_E@cat.com, Wayne.Book@me.gatech.edu

Abstract

The use of haptic interfaces to control mobile hydraulic machinery has several enhancing features over traditional human-machine interfaces comprised of joysticks/levers. This paper presents pressure and flow control schemes designed for coordinated haptic control. Typical of many small backhoes and excavators, the hydraulic system used on the test-bed is comprised of constant displacement pumps and proportional directional control valves. In this type of system, a main pressure regulator is needed to supply the other closed-centre valves with pressure and dumps the additional flow from the pump to tank. Using these valves for haptic applications requires accurate closed-loop control. The focus of this paper is on the flow control scheme. Performance of the proportional directional control valves are compared with and without pressure compensation. A velocity feedback loop is present in order to improve the accuracy of the control system. A small input dead-zone function is proposed in order to prevent a limit cycle around zero velocity caused by the valve dead-band. Coordinated motion with multiple cylinders is demonstrated.

Keywords: haptics, excavators, backhoes, coordinated motion, flow control, pressure compensation

1 Introduction

The definition of haptics is of or relating to the sense of touch or tactile. Haptic control implies that the human-machine interface can be programmed to artificially supply the user with arbitrary force sensations. Typically the haptic forces are used to relay information about the forces acting on a remote or virtual environment. A haptic interface offers several possible enhancements other than force reflection. These devices enable coordinated motion control and the ability to program virtual fixtures (Kontz et al., 2005a, Rosenberg, 1993) into the workspace. Coordinated control is a subtle, but profound, improvement over conventional hand controllers that work in joint space. Using joysticks that individually control the joints of the manipulator puts a "high perceptual and psychomotor demand" on the operator (Wallersteiner et al., 1988, Wallersteiner et al., 1993). Using coordinated motion control and a single hand controller whose motion corresponds directly to the slave manipulator reduces this mental load by doing the inverse kinematics for the operator.

This manuscript was received on 21 February 2007 and was accepted after revision for publication on 2 October 2007

The primary goal of this project is to explore how haptic interfaces can enhance the ability of novice and expert operators to control hydraulic machinery such as backhoe-loaders and hydraulic excavators. However, the focus of this paper is the hydraulic control system that will later be used for closed-loop haptic control. While hydraulic systems offer a practical application of haptic feedback, their characteristics can create control challenges. In the case of proportional directional control valves these characteristics include nonlinear valve orifice coefficients, delay, dead-band and slow dynamics. When implemented on mobile equipment, dynamics associated with the pump and primary pressure/flow control must also be considered. Closing the loop on these dynamics can also cause instabilities.

The valve dead-band is an issue of concern when closing the loop around a proportional directional control valve. One way to deal with dead-band is to use a dead-band inverse in the control. In the case of a servo valves with fast dynamics this can be achieved with good performance (Fortgang et al., 2002). Regardless of their cost, servo valves are not well suited for mobile application due their sensitivity to contamination. In the case of proportional valves the effectiveness of the dead-band inverse is limited by the dynamics of valves

(Liu and Yao, 2004, Taware et al., 2002). This is due to the dead-band nonlinearity being sandwiched between the spool dynamics and the dynamic of the rest of the hydraulic system. The inverse dead-band is located at the input and corrects the desired spool position; however, the limitation on how fast the spool can move determines how fast the desired spool position can be achieved. In turn, this limits how well the system can track a desired trajectory. One way to minimize the effect of spool dead-band and improve overall performance is to increase the responsiveness of the spool control stage. Tafazoli et al. (1996) created a custom differential PWM pilot stage that could move the spool faster in order to improve the responsiveness of the main spool used on their haptic mini-excavator.

Another factor that can limit how fast a system responds is the rate at which the main system pressure can build up (Lee and Chang, 2001). This is especially true of load-sensing systems that react to the maximum line pressures of any of the open valves. This type of design is good from an energy savings point of view, but is detrimental to closed-loop control which is necessary for haptic teleoperation (Krishnaswamy and Li, 2006, Salcudean et al., 1999, Tafazoli et al., 2002) or autonomous operation (Ha et al., 2002, Stentz et al., 1998, Vaha and Skibniewski, 1993). The system has to wait in order for pressure to build up when starting from rest and the pressure can drop and may need to build up again when the valve orifices are temporarily closed as the valves change the direction of the flow. This problem could be minimized by using a pressure regulating valve with an electronically controlled set point. The pressure can be built up as the spool moves through the dead-band.

Another factor that can compound this problem is that the pilot pressure that is used by the main spool is supplied from a pressure reducing valve that is fed by the main system pressure. When all the spools are in the dead-band region, the main system pressure can drop below the set point of the pressure reducing valve. Due to this, the spool pilot pressure drops along with the responsiveness of the spool. This problem can be address by either setting a minimum stand-by pressure or having a separate pilot system.

From an energy and performance standpoint, being able to optimize the pressure of the system is particularly important on this type of system. Typically, larger equipment such as backhoe-loaders and hydraulic excavators have variable displacements pump(s) and a separate pilot system. The variable displacement pump allows both pump flow(s) and pressure(s) to follow the demands of the task. Having a separate pilot system allows the main pump pressure to drop to a very low pressure without reducing the pilot pressure. These features are less likely to be installed on smaller machines such this tractor mounted backhoe and mini-excavators due to hardware cost and size constraints.

Flow allocation must also be considered. The main pressure regulator is essentially a pressure relief valve that is modulating the pressure of the system. In Kontz et al. (2005b) three different pressure regulating configurations were explored: the original hydro-mechanical load-sensing pressure regulator, a constant pressure relief valve and an electronic load-sensing pressure relief valve. The tests in this paper only use the electronic pressure relief valve. One thing that all three of these configurations have in common is that if they are not bypassing a sufficient amount of flow they are not able to regulate the system pressure. This can be solved by limiting the flow commanded by the controller. An electronic load-sensing scheme to control pump pressure is presented in Kontz and Book (2007).

The focus of this paper is on controlling cylinder flow rates in order to achieve coordinated motion. In the following section the experimental setup is described. In Section 3, flow control strategies are presented and analyzed. In Section 4, two trajectories are described in task-space. These simple task-space trajectories are then mapped into cylinder-space (Kontz and Book, 2006) and coordinated motion is demonstrated.

2 Experimental Setup

Fig. 1: *Georgia Tech's haptic backhoe test-bed*

The primary test-bed in this project is referred to as HEnRE (Haptically ENhanced Robotic Excavator) (Frankel, 2004) is based around a 4410 series John Deere tractor with a Model 47 backhoe and a PHANToM (Massie and Salisbury, 1994) haptic display built commercially by SensAble Technologies. The Model 47 backhoe has been modified. Originally, manual valves were the only means available to operate the device. Flow is supplied from a constant displacement pump. It has been retrofitted with Sauer-Danfoss PVG-32/PVES electro-hydraulic (EH) valves and an array of sensors for feedback control and monitoring. A mechanical valve is used to switch between the original valves and the retro-fitted EH valves. A Sun Hydraulics RPEC-8WN/RBAP-MAN-224 electro-proportional pressure relief valve was added for electronic pressure control. Instrumentation installed on HEnRE includes: position of all four degrees of freedom (swing, boom, stick and bucket), capside and rodside pressures, main supply pressure, load-sense pressure, main pump flow and inlet oil temperature. The control software for the backhoe is based on Mathwork's xPC target. This real-time control software interfaces with another computer

controlling the PHANToM via Ethernet cable using UDP protocol. PHANToM control is done in a Windows operating system using SensAble's C++ software libraries.

3 Hydraulic System and Control

The hydraulic system on this tractor can be split into three major components: a constant displacement pump, a relief valve and the four proportional control valves (Fig. 2). The PVG-32 modules are stackable and contain the main flow control spools and pressure lines. Two different versions of the PVG-32 are used in this paper. One version has pressure compensation and the other does not. Each PVG-32 module has a PVES module that measures and controls the position of the main spools using PWM controlled solenoid valves in a wheatstone bridge configuration. The input voltage to the PVES is approximately proportional to the position of the spool or the size of the spools metering orifice. With the pressure compensators maintaining a constant pressure drop across the orifice, the input voltage is also more or less proportional to the flow delivered by the valves. An electro-proportional relief valve is used to control the high side pressure of the constant displacement pump on the tractor (Kontz and Book, 2007). This pressure is the system or supply pressure, P_s, driving the proportional valves.

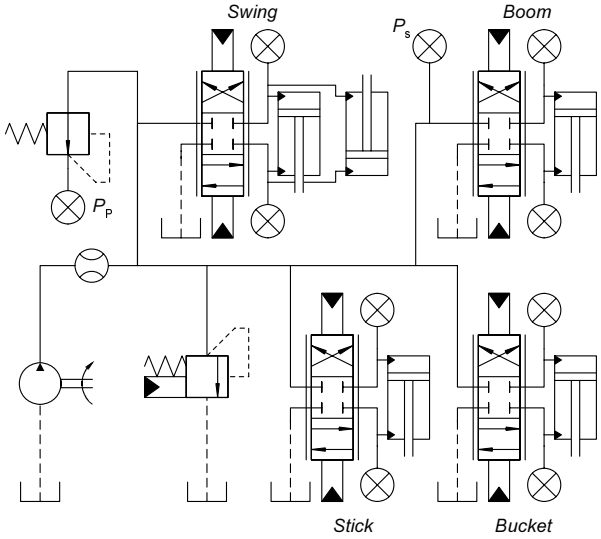

Fig. 2: *Schematic of the overall electro-hydraulic system. A pressure relief valve sets the system or pump pressure, P_s, and four proportional valves supply flow and pressure to the backhoe's cylinders. Not shown in this schematic are the PVES stages that control the motion of proportional valves. The pressure reducing valve regulates that pilot pressure, P_P, used by the PVES spool control stages*

3.1 Flow Control

One possible flow control strategy is to supply the spool directly from the pump pressure. This hardware configuration is typical of many advanced controllers found for directional proportional valves found in the literature: differential-PWM pilot control for impendence control (Tafazoli et al., 1996, Tafazoli et al., 2002), adaptive robust control (Yao et al., 2000) and passive control (Li and Krishnaswamy, 2004, Krishnaswamy and Li, 2006). An alternate hardware configuration is to use pressure compensators with the proportional spool valve. This is not a new concept (Merritt, 1967), but is still a topic of research (Kappi and Ellman, 2000, Alirand et al., 2002). Using a pressure compensator maintains a near constant pressure across the spool orifice given that the difference between the pump pressure and port pressure is greater than or equal to this value.

Using pressure compensators can be used to decouple pump pressure and port pressures in a load-sensing system (Pettersson et al., 1996, Kontz and Book, 2007).

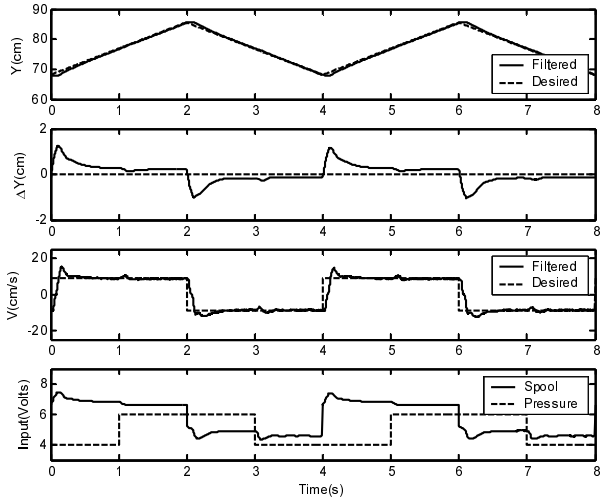

Fig. 3: *Response to saw-tooth input without a pressure compensator. Notice the small jumps in speed when the pressure input is changed. Also notice corresponding change in spool position*

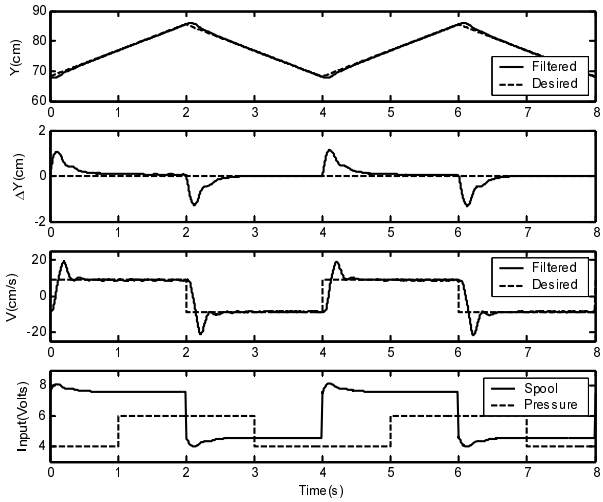

Fig. 4: *Response to saw-tooth input with a pressure compensator. There is no detectable change in either velocity or spool input when the pressure input is changed*

In addition to linearizing the relationship between spool position and flow, using a pressure compensator improves the system's reaction to changes in pressure. This was shown analytically and experimentally by Wu et al. (2007). These changes in pressure can be a result of either changes in pump pressure or load changing the port pressures. This is demonstrated by Fig. 3 - 4. In Fig. 3, the system does not have pressure compensation. In this controller, the flow command is calculated from the sum of desired velocity and a proportional position feedback term. The input to the pump pressure (dashed line in fourth subplot) is given step changes in the middle of the ramp commands. This results in a disruption to the velocity as the spool's orifice size adjusts to compensate for the disturbance and change in pressure. In Fig. 4 the same test is done with pressure compensators installed. The pressure compensators respond to the change in pressure fast enough that there is no apparent change in either input or velocity. This implies that the dynamics of the pressure compensators are much faster than the closed-loop dynamics of the spool. The only difference to the controller used in Fig. 4 is that the desired flow is fed into a look-up table relating flow rather than orifice size to input voltage. Figure 5 demonstrates the difference in flow versus the square-root of pressure differential, ΔP, for two different spool inputs. The pressure differential is defined as the pump pressure minus the port pressure.

The data without pressure compensation is nearly linear when flow is plotted versus the square-root of ΔP. With the pressure compensators installed, the flow is essentially constant for different pressures. The trend lines were generated from the respective look-up tables used in the tests shown in Fig. 3 - 4.

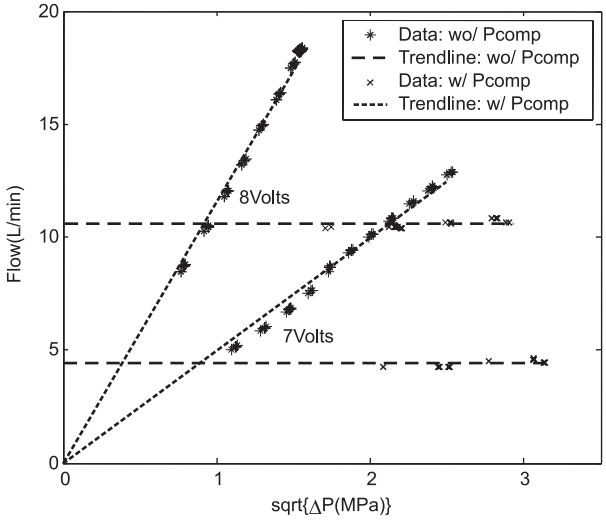

Fig. 5: *The data in this plot was taken while the bucket cylinder is extending with input voltages equal to 7 and 8 Volts. Without the pressure compensators (Pcomp) the relationship between flow and the square-root of pressure drop is linear as the orifice equation suggests. However, with the pressure compensator, the flow is nearly constant above 1 MPa (150 psi) where the pressure compensator starts to regulate the pressure drop across the orifice*

3.1.1 Pressure Compensation

Without pressure compensators, the main spool operates with no restriction between the pump and spool (Fig. 6). The relationship between flow, Q, and pressure drop across the orifice, ΔP, can be described using the orifice equation.

$$Q = C_d A_o \sqrt{\frac{2}{\rho}\Delta P} \tag{1}$$

Where C_d is the discharge coefficient and A_o is the orifice area. The combined term $C_d A_o$ is a function of spool position, x_{sp}, because the area and shape of the orifice change as the spool moves. As the temperature increases density, ρ, decreases and C_d increases due to a decrease in viscosity of the oil. Both of these factors result in more flow for the same pressure drop.

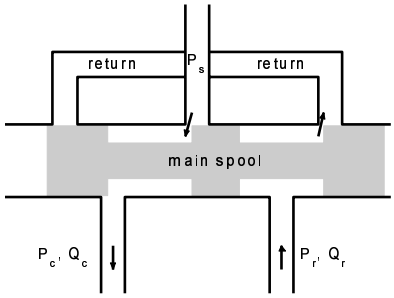

Fig. 6: *Without a pressure compensator the main spool is fed with pressure directly from pump*

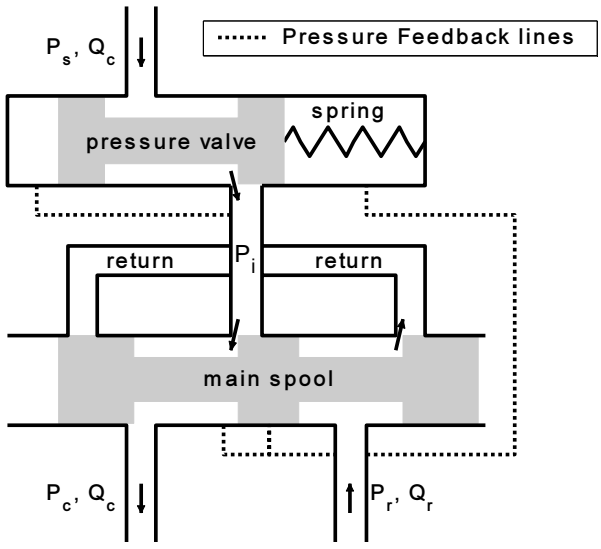

Fig. 7: *The two pressure feedback lines are used to maintain a near constant pressure drop across the metering orifice of the main spool*

As shown in Fig. 7, there is an additional two-way valve between the pump and spool that acts as the pressure compensator. The principal behind the pressure compensator is similar to that of relief and reducing valves, the two most common types of pressure valves. The governing equations of motion for a pressure compensator is similar to those presented for a pressure relief valve in Merrit (1967) and Manring (2005).

$$F_0 - A_v P_i + A_v P_p + F_x = M_v \ddot{x}_v + K_e x_v \quad (2)$$

The variable F_0 is the preload on the spool, A_v is the area of the spool, P_i is the intermediate pressure between the compensator and spool, P_p is the port pressure, F_x is the flow force, M_v is the mass of the pressure spool, K_e is equivalent stiffness and x_v is spool position. These valves are designed such that the primary forces dominating the steady-state position are directly related to pressure drop across the main spool.

$$F_0 = A_v \left(P_i - P_p \right) = A_v \Delta P \quad (3)$$

In other words, the nominal pressure differential across the main spool is F_0/A_v. Change in flow, oil temperature and pressure across the pressure spool only create a minor change in pressure drop across the main spool. Adding orifices in the pressure feedback lines is often necessary to add damping and stabilize the otherwise lightly damped dynamics of pressure valve (Kappi and Ellman, 2000, Merritt, 1967).

3.1.2 Velocity/Flow Control Law

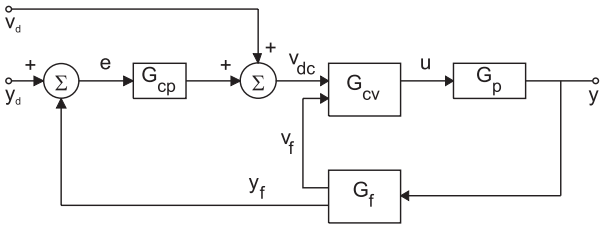

Fig. 8: *Block diagram of the overall control structure*

The primary goal of this hydraulic system is to control the motion of a manipulator. In this case, the object being controlled is the bucket of a backhoe. Kinematic mappings relate the position and orientation and their time derivatives to cylinder position and velocity and ultimately the flows produced by the valves. How the position and velocity is mapped as well as methods to deal with workspace limitations are discussed in Kontz and Book (2006). Even though the end goal is to have coordinated motion with haptic feedback, the focus here is on the hydraulic flow/speed control of the cylinders.

The general structure of the cylinder level control is shown in Fig. 8. A higher level controller specifies both cylinder position and velocity in the case of coordinated position mode or just velocity in the case of coordinated rate mode. It is assumed that both signals are available. If a proportional term is used the control law is as follows.

$$v_{dc} = v_d + K_p (y_d - y) = \dot{y}_d + K_p (y_d - y) \quad (4)$$

Assuming the dynamics of the pressure compensator are significantly faster than the valve, it is possible to ignore the complex dynamics of the pressure compensator in the control design. Judging from the test presented in Fig. 3 - 4, this is a good assumption. If v_{dc} is used to calculate the flow command the plant can be modeled as an integrator with second order dynamics.

$$G_p(s) = \frac{Y(s)}{V_{dc}(s)} = \frac{K_{flow} e^{-\tau s}}{s^3/\omega_n^2 + s^2 2\zeta/\omega_n + s} \quad (5)$$

where,

$$K_{flow} = \frac{\text{actual steady state flow}}{\text{expected steady state flow}} \quad (6)$$

In this transfer function $fn = w_n/(2\pi) \approx 7$ *Hz*, $\zeta \approx 0.7$ and $\tau = 1/80$ (half the PWM period). An approximation of the zero-order-hold in the s-domain is to add a delay equal to half the sampling time (Dorsey, 2002). The same approximation is used here for the effect of the PWM in the s-domain. This transfer function is a good approximation if the pump pressure is sufficiently higher than the setting of the reducing valve feeding the PVES spool control modules (Kontz et al., 2005b).

The flow gain, K_{flow}, includes the uncertainty in commanded flow introduced by modeling error, variations in oil temperature and pressure. It is assumed that $0 < K_{flow} < 1 + \Delta_{max}$. The pressure compensators keep this gain close to unity. In the case where pump pressure can not be increased to maintain the pressure margin, the gain could drop significantly below 1. This limits the uncertainty to $-1 < \Delta < \Delta_{max}$ where $K_{flow} = 1 + \Delta$. If the pressure compensator is working properly and is sufficiently fast, then Δ_{max} should be closer to zero than one. Using the control law in Eq. 4 and the plant transfer function in Eq. 5, the steady-state error can be found using the final value theorem. If a constant velocity input (position ramp) is given to the system the equation for steady-state position error is as follows.

$$e_{ramp} = \frac{\Delta}{(1+\Delta) K_p} \quad (7)$$

If $K_{flow} = 1$, the system will perfectly track a ramp even though it is only a Type I system (Franklin et al., 1994). This is because the velocity feed forward term is producing the nominal input signal meaning that the error is driven to zero by the position feedback.

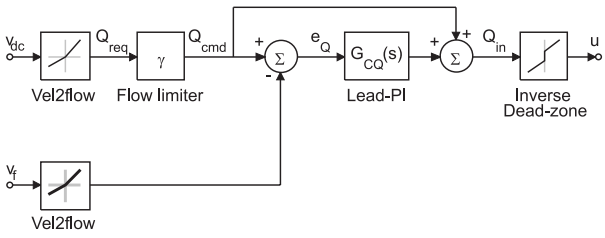

Fig. 9: *Block diagram of the velocity/flow control structure from the G_{cv} block shown in Fig. 8*

While the pressure compensator does help limit Δ it would still be good to design a controller that can track velocity with zero steady-state position error even with $\Delta \neq 0$. One way to do this is to add integral action to G_{cp}. This has two drawbacks. First, it is necessary to implement a flow limiting controller to guarantee that the pressure relief valve regulating the pump pressure can work properly (Kontz and Book, 2007). The flow gain, γ, ranges between zero and unity (Fig. 9). The gain is shared by all cylinder controllers in order to maintain the desired direction of velocity even if the

magnitude is not achievable. Second, it would be best not to integrate position error during constrained bucket motion. The alternative is to add integral action to G_{cv}. On this test-bed, only position signals are available. The block G_f is a filter that estimates both position and velocity

$$G_{fy}(s) = \frac{Y_f(s)}{Y(s)} = \frac{1}{s^2/\omega_f^2 + s\,2\zeta/\omega_f + 1} \tag{8}$$

$$G_{fv}(s) = \frac{V_f(s)}{Y(s)} = \frac{s}{s^2/\omega_f^2 + s\,2\zeta/\omega_f + 1} \tag{9}$$

The compensator chosen for G_{CQ} in Fig. 9 is a double lead-PI. The transfer function of this double-lead-PI compensator is as follows.

$$G_{CQ}(s) = K_Q\left(\frac{s^2/\omega_{zL}^2 + s\,2\zeta/\omega_{zL} + 1}{s^2/\omega_{pL}^2 + s\,2\zeta/\omega_{pL} + 1}\right)\left(\frac{s/\alpha_{PI} + 1}{s}\right) \tag{10}$$

Adding another pole at zero from the PI part of the compensator assures that that the steady-state velocity error for a constant velocity command is driven to zero error. The double-lead zeros are designed to cancel out the complex poles from the valve spools (Eq. 5) in the root locus in Fig. 10.

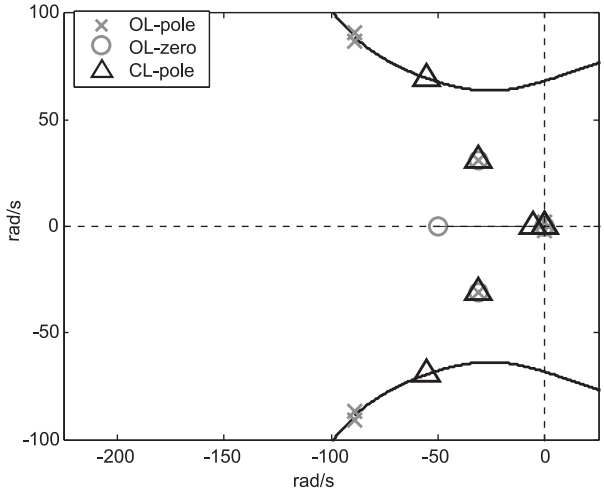

Fig. 10: *Root locus plot of dominant poles and zeros of the proportional valve, low-pass differentiator and lead-PI compensator*

The transfer function of this double-lead-PI compensator is as follows.

$$G_{CQ}(s) = K_Q\left(\frac{s^2/\omega_{zL}^2 + s\,2\zeta/\omega_{zL} + 1}{s^2/\omega_{pL}^2 + s\,2\zeta/\omega_{pL} + 1}\right)\left(\frac{s/\alpha_{PI} + 1}{s}\right) \tag{1}$$

The parameters used in this compensator are shown in Table 1.

Anti-windup was added to the integrator in order to stop the valve input from being saturated. In order to facilitate the anti-windup algorithm (Franklin et al., 1994), the PI part of this control block is separated from and placed after the lead compensator. Adding the integrator action to the inner velocity loop has the same effect as setting K_{flow} = 1 as far as steady state error is concerned. The choice of filters and compensators was designed using the Bode plot shown in Fig. 11. This Bode plot includes the dynamics from the compensator, plant and filter. Linear simulation was used to check the response and effect of sensor noise. Three things limited the achievable cutoff frequency: bandwidth of valves, delay or phase introduced by the PWM and sensor noise. The numerical values of this controller are summarized in Table 1. All of the controller transfer functions were implemented digitally using Tustin's method.

Table 1: Controller parameters

Parameters	Description	Value[units]
K_Q	Gain	5 [ ]
ω_{zL}	Lead zeros	7·2π [rad/s]
ω_{pL}	Lead poles	20·2π [rad/s]
α_{PI}	PI zero	8·2π [rad/s]
ω_f	Filter cutoff	20·2π [rad/s]
K_p	Position P-Gain	5 [1/sec]
ζ	Damping ratio	$2^{-1/2} \approx 0.7$ [ ]

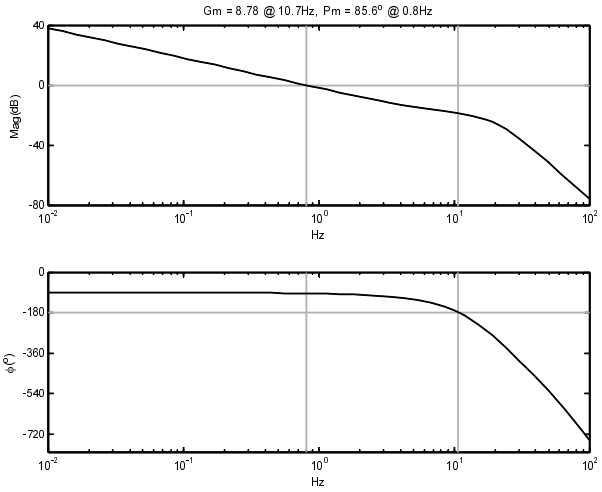

Fig. 11: *Bode plot of velocity/flow compensator, plant and low-pass differentiator*

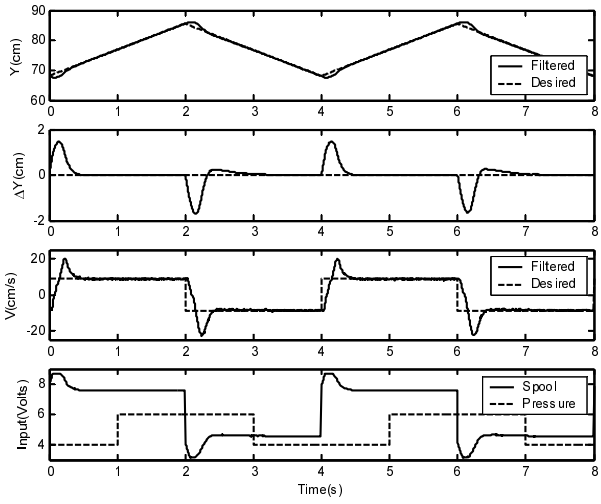

Fig. 12: *Response to saw-tooth input with pressure compensator and velocity/flow feedback with integral action. Note that there is no steady-state position error to these ramps*

As mentioned earlier, it was assumed that desired position, y_d, and velocity, v_d, were available. In the case of coordinate or resolved rate mode, only desired velocity would be received from the human-machine interface. With no position signal, K_p would be set to zero and $v_{dc} = v_d$. Using the same velocity/flow compensator without position feedback results in a loop gain between v_d and v_f that is a Type I system. This means that a step in velocity or constant velocity inputs has zero steady-state velocity error.

Linear simulations and experiments both verify the effect of Δ on performance. Positive values of Δ result in less damping and extremely negative values result in sluggish, but stable performance. The same test shown in Fig. 3 - 4 is repeated in Fig. 12 with the velocity feedback control loop. Notice that there is no steady state position error and good dynamic response.

3.1.3 Dead-band Transition

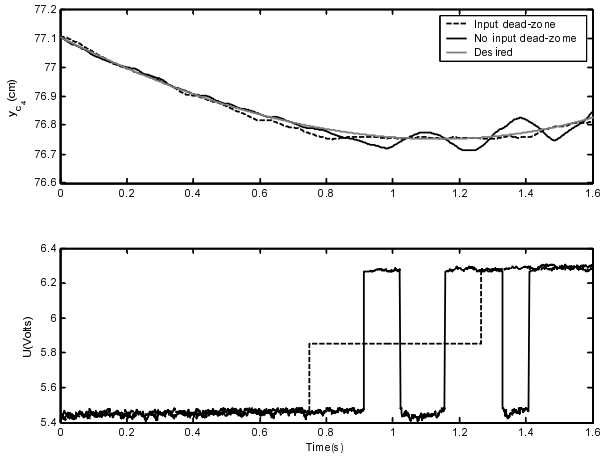

Fig. 13: *Changing cylinder direction with and without the small velocity input dead-zone*

The proportional spool valve can be approximated by two linear regions separated by a dead-band. The dead-band is designed to hold the load when flow is not being sent to either one of the ports. It also limits how fast the valve can change the direction of the flow. This makes it hard for the valve to regulate flow around zero and can lead to a limit cycle (Liu and Yao, 2004) from the dead-band nonlinearity being sandwiched between the valve and plant dynamics. This means that the valve dynamics are between the dead-band and any inverse dead-zone function used in the controller. One way to eliminate the limit cycle is to reintroduce a small dead-zone before the inverse dead-band function. This is done by modifying the cylinder input velocity, v_{dc}, using the following non-linearity.

$$v_{dc}^{*} = \begin{cases} v_{dc} - \Delta_v e^{\Delta_v (\Delta_v - v_{dc})} & \Delta_v < v_{dc} \\ 0 & -\Delta_v \le v_{dc} \le \Delta_v \\ v_{dc} + \Delta_v e^{\Delta_v (\Delta_v + v_{dc})} & v_{dc} < -\Delta_v \end{cases} \quad (12)$$

In this controller, Δ is set to *1* mm/s. This nonlinear function has almost no effect on v_{dc} at higher speeds due to the exponential terms going to zero. The down fall of this method is that it introduces some position error around zero velocity. This can be bounded by setting $v_d = 0$ in Eq. 4 and comparing to Δ.

$$|e_{zv}| \le \frac{\Delta}{K_p} \quad (13)$$

In this equation, the position error at zero velocity is bounded by $\Delta/K_p = 0.2$ mm. This is acceptable because it eliminates a limit cycle of greater amplitude. In Fig. 13, the boom cylinder is transitioning from retract to extend. With the input dead-zone, the cylinder stops and the spool is maintained in the middle of the dead-band. Without this additional non-linearity, the cylinder enters a limit cycle as the cylinder overshoots and the spool moves from one side of the dead-band to the other. Notice the delay between when the spool command is given and when the velocity or flow changes direction. Experiment using spool position feedback indicates that this delay should be on the order of 50 ms.

The output of this non-linearity is also used to decide the requested pump pressure for that particular cylinder. If the modified cylinder velocity command, v_{dc}^{*}, is zero the pump pressure request for that cylinder is also zero. Otherwise it is set to the appropriate port pressure depending on the sign of the velocity.

The integrator action is also reset to zero while $v_{dc}^{*} = 0$. This is implemented by modifying the saturation points of the nonlinearity in the anti-windup algorithm depending on the sign of v_{dc}^{*}.

4 Coordinated Motion

Two tests were conducted to demonstrate the coordinated motion of the backhoe test-bed. One moved the bucket along an arc and the other moves the bucket along a trajectory with a right angle elbow. In addition, two different controllers are used: the PI-lead and one with only the position feedback ($K_Q = 0$). The swing is kinematically decoupled from the boom, stick and bucket and is not used in these tests. This allows the trajectory to be described using the task-space cylindrical coordinates *r* and *z* and the absolute bucket angle *φ*. The cylindrical coordinates *r* and *z* describe the translational motion of the wrist of the bucket. These variables and the relationship to the cylinder-space variables are described in Fig. 14. The absolute bucket angle, *φ*, is measured from the horizontal plane and is maintained at a constant angle. Both the "Elbow" and "Arc" trajectories are plotted in Fig. 15.

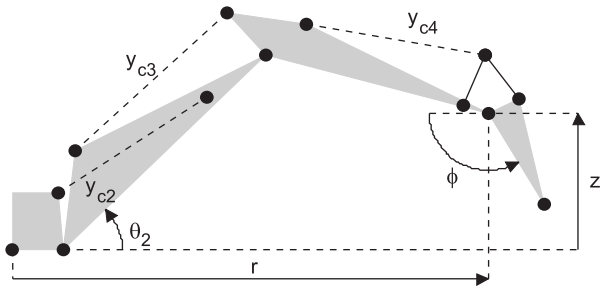

Fig. 14: *Task-space variables r, z and φ with cylinder-space variables y_{c2}, y_{c3} and y_{c4}*

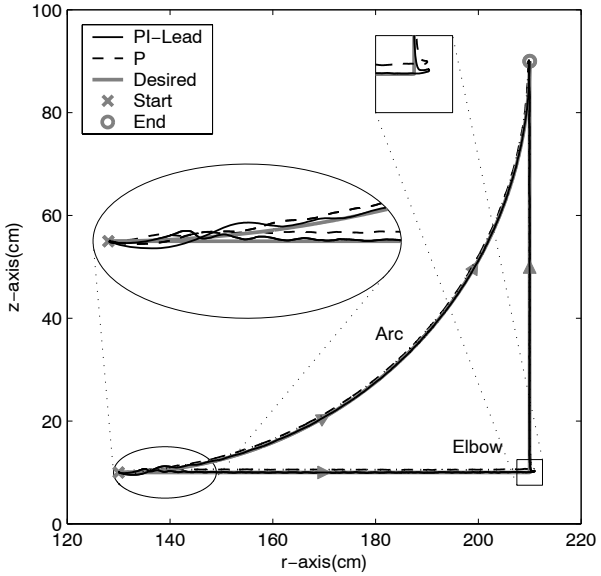

Fig. 15: *Coordinated motion in the r-z plane with the PI-lead control and P only control*

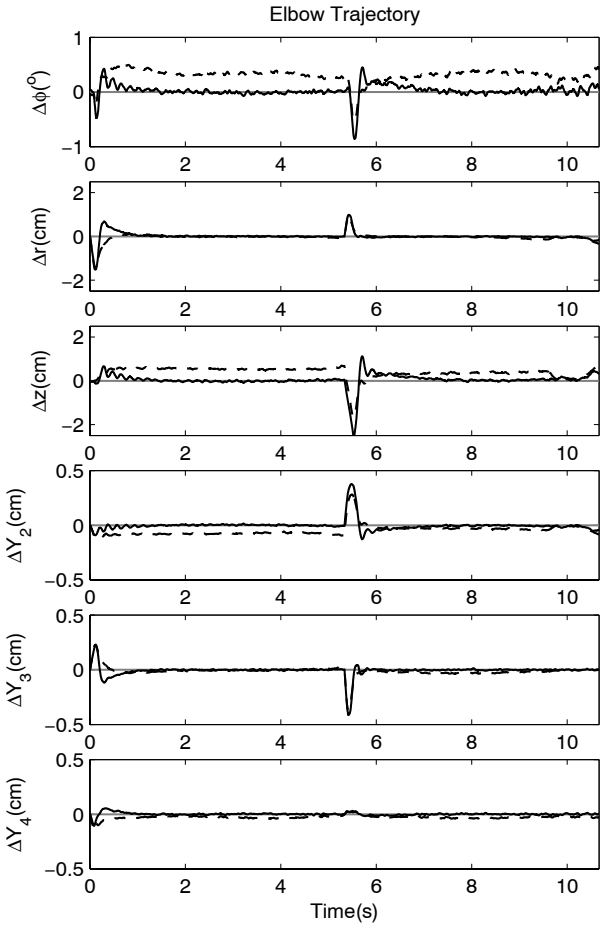

Fig. 16: *Position error vs. time for the "Elbow" trajectory. The dashed line is the response with only velocity feed forward and proportional position control*

In both cases, the backhoe starts at rest. While the desired position and velocity of these trajectories can be easily described in task space, these signals must be mapped into cylinder-space coordinates (Kontz and Book, 2006). For coordinated position mode, the desired position and velocity are mapped directly from the human-machine interface. If a more traditional rate scheme is employed, then the rate command mapped from the position of the human-machine interface is set equal to v_{dc} and K_p in Eq. 4 is set to zero, removing the position feedback loop.

Figures 16 and 17 show the error signals corresponding to the task-space coordinates (r, z and φ) and cylinder-space coordinates (y_{c2}, y_{c3} and y_{c4}) for the "elbow" and "arc" trajectories respectively.

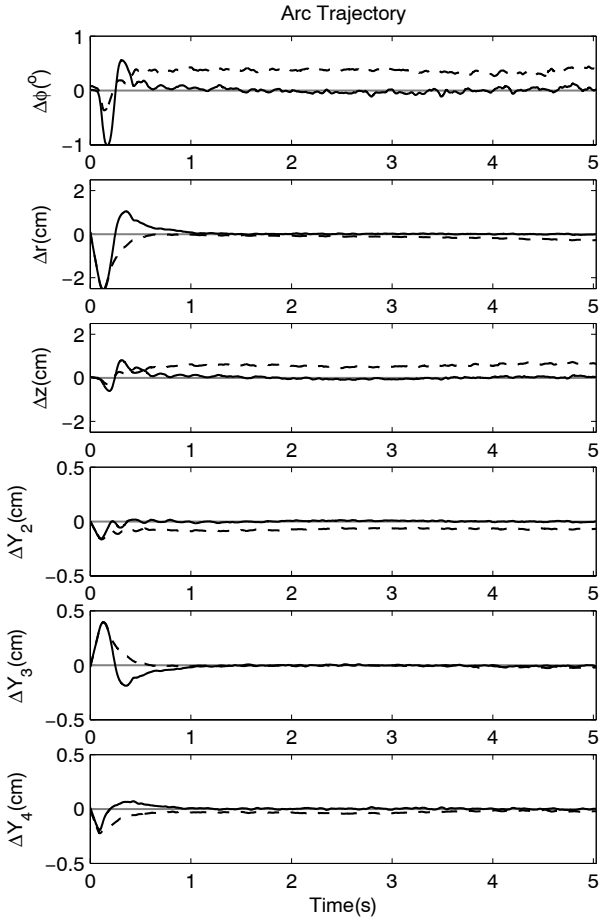

Fig. 17: *Position error vs. time for the "Arc" trajectory. The dashed line is the response with only velocity feed forward and proportional position control*

In both tests, there is some ripple in the boom cylinder as the boom starts to drop. This is probably caused by the pressure compensator going from fully open to almost completely closed. This is because the boom is over-running and another function is commanding a higher pressure from the pump. Due to gravity forces and the asymmetric cylinders, cap pressure is very low when receiving flow from the pump. Since the cylinder is above the boom, the cylinder must extend in order to lower the boom. With symmetric spools this results in a high pressure demand when raising the boom and a low pressure demand when lowering the boom. Having low pressure means that the pressure drop across the pressure compensator needs to be high. Especially at low flows, this requires the pressure compensator to be almost closed to achieve a small orifice

and work at the extreme of the compensator's design. Before the pressure compensator closes, the flow gain, K_{flow}, could be much higher than one. This drives some of the poles in the root locus towards the right-half-plane (Fig. 10). Then once the pressure compensator closes off the oscillation dies out as the flow gain return to around one.

Comparing the two controllers, it can be seen that tracking error is eliminated with the PI-lead controller. However, oscillations in the boom cylinder do not occur with the controller that only utilizes position feedback.

5 Conclusions

In this system, it was found experimentally that the system could respond faster to changes in pressure if pressure compensators were used in the circuit. This also limits the gain of the system by limiting the pressure across the spool. This simplifies the controller design. An inner velocity feedback loop is added in addition to the control incorporating only velocity feed forward and proportional position feedback. This loop is designed to improve the flow accuracy of the system and improve tracking. A small input dead-zone is proposed in order to eliminate limit cycles around zero flow. This non-linearity has no affect at higher flow and trades position around zero velocity for a limit cycle with larger amplitude. Finally, coordinated motion is demonstrated using two trajectories that are described in task-space and mapped into cylinder space.

The velocity/flow controller described in this paper as well the kinematic mappings utilized in the results will be a building block for coordinated haptic control of this backhoe test-bed.

Nomenclature

A_o	Orifice area	[m^2]
A_c	Cap (head) end area	[m^2]
A_r	Rod end area	[m^2]
A_v	Valve area	[m^2]
C_d	Discharge coefficient	[]
e	Position error	[m]
e_{zv}	Position error at zero velocity	[m]
F_o	Nominal force	[N]
F_x	Flow force	[N]
f_n	Main spool frequency	[Hz]
G_{cp}	Position controller	[]
G_{cv}	Velocity controller	[]
G_{CQ}	Velocity/flow compensator	[]
G_y	Filter	[]
G_{fy}	Position filter	[]
G_{fv}	Velocity filter	[]
K_e	Equivalent stiffness	[N/m]
K_{flow}	Flow gain	[]
K_Q	Flow controller gain	[N/m]
K_p	Position P-gain	[N/m]
M_v	Valve mass	[kg]
P	Pressure	[Pa]
P_s	Supply/system pressure	[Pa]
P_c	Cap end pressure	[Pa]
P_i	Intermediate pressure	[Pa]
P_p	Port (cap or rod) pressure	[Pa]
P_r	Rod end pressure	[Pa]
ΔP	Pressure drop	[Pa]
Q	Flow	[m^3/s]
Q_c	Flow to cap end	[m^3/s]
Q_r	Flow to rod end	[m^3/s]
v	Actual velocity	[m/s]
v_d	Desired velocity	[m/s]
v_{dc}	Desired corrected velocity	[m/s]
x_v	Spool position	[m]
y	Cylinder displacement	[m]
y_d	Desired cylinder displacement	[m]
α_{PI}	PI zero	[rad/s]
ζ	Damping ratio	[]
Δ	Uncertainty	[]
Δ_v	Velocity input deadzone	[m/s]
ρ	Density	[kg/m^3]
ω_n	Main spool frequency	[rad/s]
ω_f	Filter cutoff frequency	[rad/s]

Acknowledgements

This work is partially supported through HUSCO International, John Deere and the other supporting companies of the Fluid Power and Motion Control Center of Georgia Tech.

References

Alirand, M., **Favennec, G.** and **Lebrun, M.** 2002. Pressure Components Stability Analysis: A Revisited Approach. *Intl. Journal of Fluid Power,* 3(1), pp. 33-45.

Dorsey, J. 2002. *Continuous and Discrete Control Systems.* New York, NY. McGraw-Hill

Fortgang, J. D., **George, L. E.** and **Book, W. J.** 2002. Practical implementation of a dead zone inverse on a hydraulic wrist. *Intl. Mech. Engr. Congr. Expo., FPST-Vol 9, ASME New Orleans, LA*, pp. 149-155.

Frankel, J. G. 2004. *Development of a Haptic Backhoe Testbed.* M.S. Thesis, G.W. Woodruff School of Mechanical Engineering. Georgia Institute of Technology.

Franklin, G. F., **Powell, J. D.** and **Emani-Naeini, A.** 1994. *Feedback Control of Dynamic Systems.* Reading, MA. Addison-Wesley.

Ha, B. Q., **Santos, M.**, **Nguyen, Q.**, **Rye, D.** and **Durrant-Whyte, H.** 2002. Robotic excavation in construction automation. *IEEE Robotics and Automation Magazine,* 9(1), pp. 20-28.

Kappi, T. J. and **Ellman, A. U.** 2000. Analytical method for defining pressure compensator dynam-

ics. *Intl. Mech. Engr. Congr. Expo., FPST-Vol 7, ASME*, Orlando, FL, pp. 121-125.

Kontz, M. E., **Beckwith, J.** and **Book, W. J.** 2005a. Evaluation of a teleoperated haptic forklift. *Intl. Conference on Advanced Intelligent Mechatronics, IEEE/ASME*, Monterey, CA, pp. 295-300.

Kontz, M. E., **Huggins, J. D.**, **Book, W. J.** and **Frankel, J. G.** 2005b. Improved Control of Open-center Systems for Haptics Applications. *Intl. Mech. Engr. Congr. Expo.*, DSC-Vol 74-1A, ASME, Orlando, FL, pp. 823-831.

Kontz, M. E. and **Book, W. J.** 2006. Kinematic Analysis of Backhoes/Excavators for Closed-loop Coordinated Control. *Proc. Intl. Symp. Robot Control*, Bologna, Italy.

Kontz, M. E. and **Book, W. J.** 2007. Electronic Control of Pump Pressure for a Small Haptic Backhoe. *Intl. Journal Fluid Power,* 8(2), pp. 5-16.

Krishnaswamy, K. and **Li, P. Y.** 2006. Bond graph based approach to passive teleoperation of a hydraulic backhoe. *ASME J. Dyn. Syst. Meas. and Control,* 128(1), pp. 176-85.

Lee, S.-U. and **Chang, P. H.** 2001. Control of a heavy-duty robotic excavator using time delay control with switching action with integral sliding surface. *Proc. Intl. Conf. on Robotics and Automation, IEEE*, Seoul, South Korea, pp. 3955-60.

Li, P. Y. and **Krishnaswamy, K.** 2004. Passive Bilateral Teleoperation of a Hydraulic Actuator using an Electrohydraulic Passive Valve. *Intl. Journal Fluid Power,* 5(2), pp. 43-56.

Liu, S. and **Yao, B.** 2004. Programmable valves: a solution to bypass deadband problem of electro-hydraulic systems. *Proc. American Control Conf.*, Boston, MA, pp. 4438-43.

Manring, N. D. 2005. *Hydraulic Control Systems.* Hoboken, NJ. John Wiley and Sons, Inc.

Massie, T. H. and **Salisbury, K. J.** 1994. PHANToM haptic interface: a device for probing virtual objects. *Intl. Mech. Engr. Congr. Expo.*, DSC-Vol 55-1, ASME, Chicago, IL, pp. 295-299.

Merritt, H. E. 1967. *Hydraulic Control Systems.* New York. Wiley.

Pettersson, H., **Krus, P.**, **Jansson, A.** and **Palmberg, J.-O.** 1996. The Design of Pressure Compensators for Load Sensing Hydraulic Systems. *Proc. Int. Conf. Control*, London, UK, pp. 1456-1461.

Rosenberg, L. B. 1993. Virtual fixtures: perceptual tools for telerobotic manipulation. *Proc. Virtual Reality Annual Intl. Symp., IEEE*, Seattle, WA, pp. 76-82.

Salcudean, S. E., **Hashtrudi-Zaad, K.**, **Tafazoli, S.**, **Dimaio, S. P.** and **Reboulet, C.** 1999. Bilateral matched impedance teleoperation with application to excavator control. *IEEE Control Systems Magazine,* 19(6), pp. 29-37.

Stentz, A., **Bares, J.**, **Singh, S.** and **Rowe, P.** 1998. A robotic excavator for autonomous truck loading. Proc. *Intl. Conf. on Intelligent Robots and Systems. , IEEE*/RSJ Victoria, BC, Canada, pp. 1885-93.

Tafazoli, S., **Peussa, P.**, **Lawrence, P. D.**, **Salcudean, S. E.** and **De Silva, C. W.** 1996. Differential PWM Operated Solenoid Valves in the Pilot Stage of Mini Excavators: Modeling and Identification. *Intl. Mech. Engr. Congr. Expo.*, FPST-Vol. 3, ASME, Atlanta, GA, pp. 93-99.

Tafazoli, S., **Salcudean, S. E.**, **Hashtrudi-Zaad, K.** and **Lawrence, P. D.** 2002. Impedance control of a teleoperated excavator. *IEEE Trans. Control Systems Technology,* 10(3), pp. 355-367.

Taware, A., **Tao, G.** and **Teolis, C.** 2002. Design and analysis of a hybrid control scheme for sandwich nonsmooth nonlinear systems. *IEEE Tran. Automatic Control,* 47(1), pp. 145-150.

Vaha, P. K. and **Skibniewski, M. J.** 1993. Cognitive force control of excavators. *J. Aerospace Engineering,* 6(2), pp. 159-166.

Wallersteiner, U., **Stager, P.** and **Lawrence, P.** 1988. A human factors evaluation of teleoperator hand controllers. *Proc. Intl. Symp. Teleoperation and Control*, Bristol, UK, pp. 291-6.

Wallersteiner, U., **Lawrence, P.** and **Sauder, B.** 1993. Human factors evaluation of two different machine control systems for log loaders. *Ergonomics,* 36(8), pp. 927-934.

Wu, D., **Burton, R.**, **Schoenau, G.** and **Bitner, D.** 2007. Analysis of a Pressure-Compensated Flow Control Valve. *ASME J. Dyn. Syst. Meas. and Control,* 129(1), pp. 203-211.

Yao, B., **Bu, F.**, **Reedy, J.** and **Chiu, G. T.-C.** 2000. Adaptive Robust Control of Single-Rod Hydraulic Actuators: Theory and Experiments. *IEEE/ASME Trans. Mechatronics,* 5(1), pp. 79-91.

Matthew E. Kontz
He received a B.S.E. from Walla Walla College in 2001 and a M.S.M.E in 2002 from the Georgia Institute of Technology. By the end of 2007, he plans to begin a career at Caterpillar and receive both a M.S. in Electrical Engineering and Ph.D. in Mechanical Engineering from Georgia Tech. His graduate research has centered on haptic control of hydraulic machinery. Prior industrial experience includes internships at Honeywell and Caterpillar and independent consulting for Ross Controls. He was the primary author on the paper receiving the 2005 ASME IMECE FPST Division Best Paper Award.

Wayne J. Book
After he received his Ph.D. degree in mechanical engineering from the Massachusetts Institute of Technology in 1974, Wayne Book joined the faculty of Mechanical Engineering at the Georgia Institute of Technology. He is currently the HUSCO/Ramirez Distinguished Professor in Fluid Power and Motion Control. His research includes the design, dynamics and control of high speed, lightweight motion systems, robotics, fluid power and haptics. He is a Fellow of both the ASME, IEEE and SME, and received the ASME Dedicated Service Award in 2003 and the ASME DSCD Leadership Award in 2004.